JACC: BASIC TO TRANSLATIONAL SCIENCE VOL. 11, NO. 2, 2026

ORIGINAL RESEARCH - PRECLINICAL

OPA1 Deficiency Impairs NGF Signaling and Drives Sympathetic Neurodegeneration

Marco Ronfini, PhD,[a,b,*] Valentina Prando, PhD,[a,b,*] Vittoria Di Mauro, PhD,[a,b] Lolita Dokshokova, PhD,[a,b] Erika Lazzeri, PhD,[c] Irene Costantini, PhD,[c,d,e] Lukas Alàn, PhD,[b,f] Erwan Andre Riviere, PhD,[b,f] Alex Incensi, BSc,[g] Camilla Olianti, PhD,[c] Chiara La Morgia, MD, PhD,[g,h] Rocco Liguori, MD,[g,h] Leonardo Sacconi, PhD,[i,j] Vincenzo Donadio, MD, PhD,[g,h] Luca Scorrano, MD, PhD,[b,f] Valerio Carelli, MD, PhD,[g,h] Marco Mongillo, MD, PhD,[a,b,k,l,†] Tania Zaglia, PhD[a,b,l,†]

VISUAL ABSTRACT

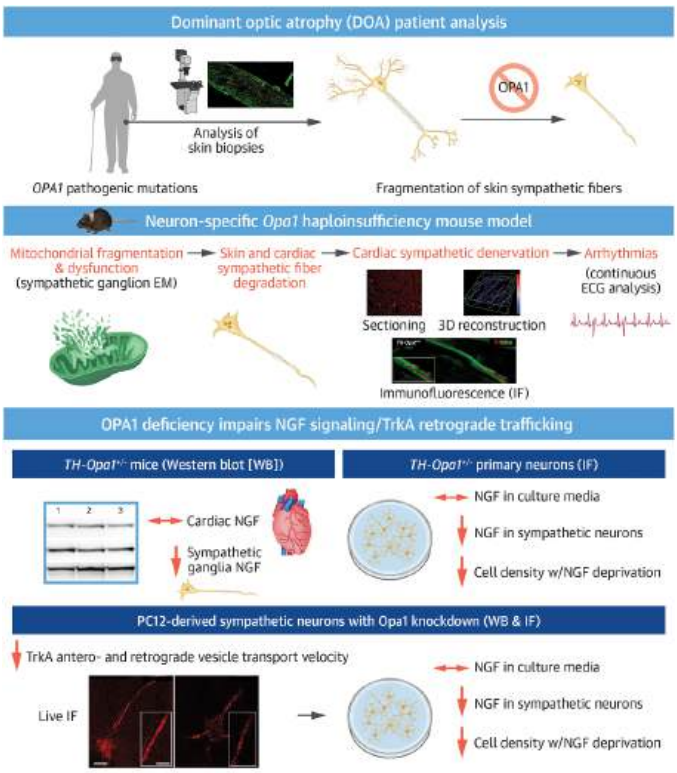

Ronfini M, et al. JACC Basic Transl Sci. 2026;11(2):101460.

HIGHLIGHTS

- **Sympathetic neurodegeneration contributes to cardiac dysfunction in dominant optic atrophy, uncovering a neuro-cardiac component of disease.**
- **Neuron-specific *Opa1* haploinsufficiency (*TH-Opa1*$^{+/-}$) reproduces the sympathetic neuron defect, showing that OPA1 loss in sympathetic neurons is sufficient to induce denervation and arrhythmias.**
- **OPA1 deficiency alters mitochondrial dynamics and impairs NGF/TrkA signaling, leading to sympathetic neuron vulnerability.**
- **Modulating mitochondrial fission (*Drp1* silencing) rescues neuronal morphology, pointing to mitochondrial dynamics as a mechanistic target.**
- **Cutaneous sympathetic fiber loss provides a potential biomarker, whereas future studies should clarify mechanisms of neurocardiac crosstalk and therapeutic opportunities.**

From the [a]Department of Biomedical Sciences, University of Padova, Padova, Italy; [b]Veneto Institute of Molecular Medicine, Padova, Italy; [c]European Laboratory for Non-linear Spectroscopy, University of Florence, Florence, Italy; [d]National Institute of Optics, National Research Council, University of Florence, Florence, Italy; [e]Department of Biology, University of Florence, Italy; [f]Department of Biology, University of Padova, Italy; [g]IRCCS Istituto delle Scienze Neurologiche di Bologna, Bologna, Italy; [h]Department of Biomedical and Neuromotor Sciences, University of Bologna, Bologna, Italy; [i]Institute of Clinical Physiology, National Research Council, Florence, Italy; [j]Institute for Experimental Cardiovascular Medicine, University Heart Center and

ISSN 2452-302X https://doi.org/10.1016/j.jacbts.2025.101460

ABBREVIATIONS AND ACRONYMS

cSN = cardiac sympathetic neuron

DOA = dominant optic atrophy

ENDO = sub-endocardium

EPI = sub-epicardium

NGF = nerve growth factor

OPA1 = optic atrophy factor-1

TH = tyrosine hydroxylase

TrkA = tropomyosin receptor kinase A

SUMMARY

Peripheral sympathetic neurodegeneration drives cardiac dysfunction in dominant optic atrophy, revealing a critical neuro-cardiac link. Optic atrophy factor-1 haploinsufficiency disrupts mitochondrial dynamics and neurotrophic signaling, causing targeted sympathetic denervation and arrhythmias. Restoring nerve growth factor transport and mitochondrial health in sympathetic neurons represents a promising therapeutic avenue for cardiac autonomic disorders. Future research must unravel mechanisms of neurocardiac crosstalk to develop precise interventions against neurogenic cardiac disease progression. (JACC Basic Transl Sci. 2026;11:101460)

The dynamin-related guanosine diphosphatase (GTPase) optic atrophy factor-1 (OPA1) is an inner mitochondrial membrane protein involved in the regulation of mitochondrial dynamics.[1] Mutations in *OPA1*, often leading to haploinsufficiency, are responsible for the majority of cases of dominant optic atrophy (DOA), the most common form of inherited mitochondrial optic neuropathy, with a prevalence of ~1 in 25,000 individuals.[2] Beyond classic DOA, the phenotypic spectrum of *OPA1* mutations, including biallelic variants, extends to early-onset encephalopathies, resembling Leigh syndrome,[3] complex multisystem disorders with cardiomyopathy[4-6] and peripheral neuropathy, and neurodegenerative features such as Parkinsonism and dementia. This broader presentation is collectively referred to as the DOA-plus phenotype.[7,8]

Although most DOA patients harbor mutations causing haploinsufficiency, missense variants, particularly within the GTPase domain, are more frequent in DOA-plus cases and are thought to exert dominant-negative effects. Nevertheless, several of these variants also reduce OPA1 protein levels, indicating that haploinsufficiency may remain a relevant pathogenic mechanism.[6,9-12] Supporting this, re-expression of DOA-plus-associated missense variants in *Opa1* knockout murine embryonic fibroblasts mimics the null phenotype.[8] These findings underscore that OPA1 dysfunction disrupts mitochondrial dynamics across multiple neuronal subtypes.[13] Mouse and *Drosophila* models have been instrumental in recapitulating the human DOA phenotype, revealing that OPA1 dysfunction can also lead to cardiomyopathy, arrhythmias, and impaired chronotropic response—features not easily explained by optic neuropathy alone.[14-18] Although these cardiac manifestations are typically ascribed to mitochondrial defects in cardiomyocytes,[5,19-22] evidence suggests that dysregulation of neurocardiac pathways may also contribute.[4,14-18] This is supported by signs of autonomic dysfunction and peripheral neuropathy in DOA-plus patients.[12,13,23-27] To test this hypothesis, we generated a mouse model with *Opa1* haploinsufficiency restricted to tyrosine hydroxylase (TH)-expressing neurons. This model enabled investigation of OPA1 deficiency specifically in cardiac and peripheral sympathetic neurons (SNs). By integrating data from this *TH-Opa1*$^{+/-}$ model with analysis of sympathetic innervation in skin biopsy specimens from DOA patients, we identified SNs as novel and functionally relevant targets in DOA pathogenesis. Mechanistically, OPA1 deficiency disrupted neurotrophic nerve growth factor (NGF)/tropomyosin receptor kinase A (TrkA) signaling, indicating impaired mitochondrial dynamics as a contributor to sympathetic neurodegeneration and highlighting candidate pathways for therapeutic neuroprotection. From a translational perspective, the detection of sympathetic fiber loss in skin biopsy specimens also suggests a minimally invasive approach to identify autonomic involvement in DOA at early disease stages.

Medical Faculty, University of Freiburg, Freiburg, Germany; [k]CNR Institute of Neuroscience, Padova, Italy; and the [l]Interdepartmental Research Center of Myology (cirMYO), Padova, Italy. *These authors contributed equally as first authors. †These authors contributed equally as last authors.

The authors attest they are in compliance with human studies committees and animal welfare regulations of the authors' institutions and Food and Drug Administration guidelines, including patient consent where appropriate. For more information, visit the Author Center.

Manuscript received July 16, 2025; revised manuscript received December 6, 2025, accepted December 9, 2025.

METHODS

HUMAN SAMPLES. Skin biopsy specimens were obtained from 12 patients carrying pathogenic *OPA1* mutations, diagnosed with either DOA or DOA-plus, and from 12 age- and sex- matched healthy controls. All participants provided written informed consent. The study was approved by the local ethics committee (Comitato Etico Indipendente AUSL Bologna; protocol code: 12073).

ETHICAL APPROVAL. All animal procedures were approved by the Italian Ministry of Health (Ufficio VI) in accordance with national Animal Welfare Legislation (protocols VIMM C-53 and C-54). Animals were housed in individually ventilated cages in an authorized facility (authorization number 175/2002A), under a 12:12 hours light/dark cycle at controlled temperature, with ad libitum access to food and water. All procedures were performed by trained personnel with certified experience in animal handling and care. Experimental protocols were refined before study initiation, and the number of animals was calculated to ensure statistical power while minimizing use.

ANIMAL MODELS. Mice expressing Cre recombinase under the control of the TH promoter (B6.129X1-Th<tm1(cre)Te>/Kieg; EMMA Laboratories)[28] were backcrossed with loxP-*Opa1* transgenic mice.[29] *TH-Cre*$^{+/-}$ and loxP-*Opa1*$^{+/+}$ lines were used for colony maintenance. For this study, adult (6-month-old) and aged (24-month-old) *TH-Opa1*$^{+/-}$ mice were analyzed. Age-matched littermates served as controls. Both male and female mice were evaluated and showed comparable results; for clarity and consistency, only male data are presented in the figures.

STATISTICS. Statistical analyses were performed using GraphPad Prism version 8.0 (GraphPad Software). Data are presented as mean ± SD. Normality was evaluated using the Shapiro-Wilk test. For 2-group comparisons, unpaired Student's *t*-tests were used for normally distributed data with equal variances; Welch's correction was applied when variances were unequal. The Mann-Whitney test was used for non-normally distributed data. One-way analysis of variance (ANOVA) was used to compare 3 or more groups with a single factor, and Brown-Forsythe ANOVA was applied when variances were unequal. The Kruskal-Wallis test was used to compare 3 or more groups that were not normally distributed. Two-way ANOVA was used for comparisons involving 2 factors. Post hoc tests for multiple pairwise comparisons, including Sidak, Tukey, and Dunnett, are detailed in the respective figure legends. For tetramethylrhodamine analyses, group differences were assessed by comparing the slopes obtained from linear regression of fluorescence intensity across the interval between oligomycin addition (2 minutes) and carbonyl cyanide-p-trifluoromethoxyphenylhydrazone treatment (38 minutes). A P value <0.05 was considered statistically significant.

A full description of experimental procedures is available in the Supplemental Material.

RESULTS

CUTANEOUS SYMPATHETIC DENERVATION IN DOA PATIENTS. Sympathetic innervation of sweat glands and arrector pili muscles can be reliably evaluated in humans through skin biopsy, a minimally invasive and validated method for assessing peripheral autonomic neurons.[30] Using this approach, we analyzed the morphology and density of peripheral SNs in skin punch biopsy specimens obtained from the thigh and lower leg of 12 DOA patients (20-70 years of age) from 8 unrelated families. All patients carried heterozygous pathogenic *OPA1* variants, mainly missense mutations linked to classical or DOA-plus phenotypes (**Figure 1A**); no compound heterozygotes were included.[6,31-33] Notably, several of these mutations have been previously reported to reduce OPA1 protein levels. To assess sympathetic innervation, we performed confocal immunofluorescence on skin sections using TH as a marker for sympathetic fibers.[34] Compared to age- and sex-matched healthy controls, DOA patient samples exhibited a marked reduction in sympathetic fiber density (TH-labeled area/tissue area [%]) in both biopsy sites (leg: 16.54 ± 2.67 in controls vs 7.57 ± 4.98 in patients, $P < 0.001$; thigh: 16.38 ± 4.09 vs 11.65 ± 4.67, $P = 0.031$). Residual fibers were noticeably thinner and fragmented, consistent with ongoing sympathetic neurodegeneration (**Figures 1B to 1D**).

GENERATION OF SYMPATHETIC NEURON-SPECIFIC *OPA1* HAPLOINSUFFICIENT MICE. To assess the effects of *Opa1* haploinsufficiency specifically in SNs, we generated mice with SN-specific *Opa1* deletion by crossing *Opa1*$^{flx/flx}$ mice with transgenic mice expressing Cre recombinase under control of the TH promoter (*TH-Cre; Opa1*$^{+/flx}$). The resulting double-heterozygous mice (*TH-Opa1*$^{+/-}$) were viable, fertile, and exhibited normal lifespan. Western blot analysis showed a 50% reduction of OPA1 protein levels (Ctrl: 1.00 ± 0.18 vs *TH-Opa1*$^{+/-}$: 0.46 ± 0.28, $P = 0.047$) in the superior and stellate ganglia, which house the soma of cardiac SNs (cSN) (**Fig.2A**).[35] *Opa1* mRNA and protein levels were unaltered in non-neuronal

FIGURE 1 **Sympathetic Denervation in Skin Biopsy Specimens From DOA Patients**

A

Family	Patient	Mutation	Aplo/ Missense	Phenotype	EMG
#1	#1	c.1462A>G (p.Gly488Arg)	Missense	CPEO + OA + PNP	PNP
#1	#2	c.1462A>G (p.Gly488Arg)	Missense	CPEO + OA + PNP + myopathy + parkinsonism + dementia	PNP
#2	#3	c.1463G>C (p.Gly488Ala)	Missense	OA + deafness	No PNP
#3	#4	c.1484C>T (p.Ala495Val)	Missense	CPEO + OA + PNP	PNP
#4	#5	c.1316G>T (p.Gly439Val)	Missense	CPEO + OA + + PNP + myopathy + mixed ataxia + deafness	PNP
#5	#6	c.1334G>A (p.Arg445His)	Missense	OA + PNP + deafness	PNP
#5	#7	c.1334G>A (p.Arg445His)	Missense	OA + deafness	No PNP
#6	#8	c.703C>T (p.Arg235Ter)	Missense	CPEO + OA	No PNP
#7	#9	c.893G>A (p.Ser298Asn)	Missense	OA + PNP + deafness myopathy + parkinsonism	PNP
#8	#10	c.2341C>T (p.Arg781Trp)	Missense	Asymptomatic (including OCT normal)	NA
#8	#11	c.751delG (p.D251MfsX13)	Haplo	Mild OA	NA
#8	#12	c.2341C>T (p.Arg781Trp)c.751delG (p.D251MfsX13)	Missense + Haplo	OA	NA

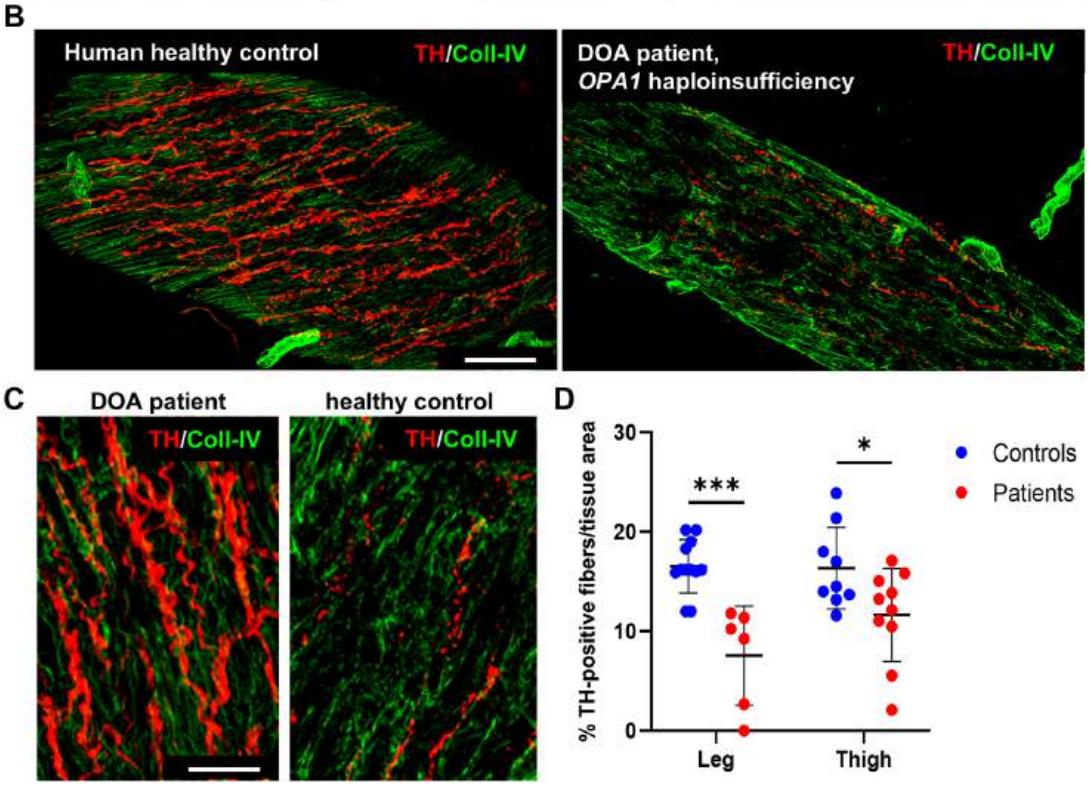

Continued on the next page

tissues, including liver, skeletal muscle, and myocardium, confirming tissue specificity. Importantly, overall mitochondrial content was unchanged, as assessed by TOM20 protein levels normalized to TH in sympathetic ganglia extracts (**Figure 2B**) (Ctrl: 1.00 ± 0.55 vs *TH-Opa1*$^{+/-}$: 1.29 ± 0.49, $P = 0.49$), indicating that OPA1 deficiency does not affect organelle abundance. By contrast, ultrastructural examination revealed mitochondrial structural abnormalities, including a significant reduction in cristae density (**Figures 2C and 2D**) (Ctrl: 5.48 ± 3.18 vs *TH-Opa1*$^{+/-}$: 3.06 ± 1.89, $P < 0.001$). TH-restricted *Opa1* haploinsufficiency did not affect gross cardiac morphology or basal contractility, which remained comparable to wild-type controls at both 6 and 24 months of age (Supplemental Figure 1) (fractional shortening: Ctrl: 31.52 ± 5.75 vs *TH-Opa1*$^{+/-}$: 33.47 ± 2.11, $P = 0.45$; ejection fraction: Ctrl: 62.96 ± 7.30 vs *TH-Opa1*$^{+/-}$: 66.05 ± 4.27, $P = 0.39$), confirming the absence of a cardiac-autonomous phenotype. Electrocardiographic (ECG) recordings in conscious mice also showed no significant differences in heart rate or QRS morphology across all age groups (Supplemental Figure 2). Remarkably, immunofluorescence analysis of TH-positive fibers in the skin revealed severe morphological abnormalities and near-complete loss of sympathetic innervation as early as 6 months (**Figures 2E and 2F**) (Ctrl: 31.08 ± 7.71 vs *TH-Opa1*$^{+/-}$: 1.33 ± 2.39, $P < 0.001$). This closely mirrored the sympathetic denervation observed in DOA patient biopsy specimens (**Figures 1B to 1D**), suggesting that OPA1 haploinsufficiency – whether due to missense or loss-of-function variants – compromises peripheral SN viability and structural maintenance.

EARLY SYMPATHETIC DEGENERATION AND ARRHYTHMIAS IN *TH-OPA1*$^{+/-}$ MICE. To investigate the functional and structural consequences of *Opa1* haploinsufficiency in cSN, we first assessed basal sympathetic activity by evaluating heart rate responses to atropine[34] (2 mg/kg, intraperitoneal injection), a muscarinic receptor antagonist that suppresses parasympathetic input. In control mice, atropine elicited the expected positive chronotropic effect, whereas *TH-Opa1*$^{+/-}$ mice exhibited a significantly blunted heart rate increase as early as 6 months of age (**Figure 3A**) (Ctrl: 28.23 ± 0.99 vs *TH-Opa1*$^{+/-}$: 9.38 ± 4.52, $P = 0.001$). A similar impairment was observed in aged animals (percentage heart rate increase: Ctrl: 16.15 ± 8.91 vs *TH-Opa1*$^{+/-}$, 6.50 ± 2.34; n = 6 per group; $P < 0.001$). Moreover, continuous ECG monitoring in freely moving mice revealed a higher incidence of premature ventricular contractions (PVCs) in both adult and aged *TH-Opa1*$^{+/-}$ mice under basal conditions (**Figures 3B and 3C**) (Ctrl: 0.92 ± 0.61 vs *TH-Opa1*$^{+/-}$: 4.95 ± 2.60; $P = 0.012$). This functional impairment prompted investigation of the underlying structural correlates in cardiac innervation. Consistent with prior studies,[34,36] reduction of myocardial sympathetic innervation (~30% reduction) and fiber fragmentation were observed in wild-type hearts during aging (**Figures 4A to 4D**) (adult: 1.51 ± 0.67 vs aged: 1.10 ± 0.58; $P = 0.009$). Remarkably, sympathetic denervation was significantly more severe in *TH-Opa1*$^{+/-}$ mice, with ~60% reduction in ventricular sympathetic fiber density already at 6 months (Ctrl: 1.51 ± 0.67 vs *TH-Opa1*$^{+/-}$: 0.63 ± 0.25; $p < 0.001$). In 24-month-old *TH-Opa1*$^{+/-}$ mice, the ventricular myocardium showed near-complete denervation. Notably, the combination of OPA1 reduction and aging caused a further ~40% loss in SN density (**Figure 4**) (Ctrl: 1.10 ± 0.58 vs *TH-Opa1*$^{+/-}$: 0.37 ± 0.23; $P < 0.001$), highlighting a synergistic effect between genetic vulnerability and age. Importantly, no changes in the morphology or density of parasympathetic fibers were detected in different heart regions at any age (subepicardium [Epi]: Ctrl: 0.49 ± 0.0.14 vs *TH-Opa1*$^{+/-}$: 0.44 ± 0.08, $P = 0.24$; sub-endocardium [Endo]: Ctrl: 0.16 ± 0.06 vs *TH-Opa1*$^{+/-}$: 0.16 ± 0.09; $P = 0.97$) (Supplemental Figure 3), supporting the specificity of TH-driven genetic manipulation and the selective vulnerability of SNs. Together, these findings demonstrate that OPA1 reduction directly induces

FIGURE 1 Continued

(A) Patient cohort analyzed in this study included 12 patients carrying pathogenic mutations in the *OPA1* gene and affected with either dominant optic atrophy (DOA) or DOA plus. (B) Confocal immunofluorescence on sections of skin biopsy specimens from a healthy human control (left panel) and a DOA patient with *OPA1* haploinsufficiency (right panel). Sections were co-stained with antibodies to tyrosine hydroxylase (TH) and collagen-VI (coll-VI). Scale bar: 30 mm. (C) Higher-magnification insets from images in (B) showing fragmentation of sympathetic fibers. Scale bar: 15 mm. (D) Quantification of sympathetic innervation density in skin biopsy specimens from healthy subjects vs DOA patients. Differences between groups were determined using Student's *t*-test (leg: n = 12 controls vs n = 6 patients; thigh: n = 9 controls vs n = 10 patients). Bars represent mean ± SD. *$P < 0.05$; ***$P < 0.001$. CPEO = chronic progressive external ophthalmoplegia; EMG = electromyography; NA = not available; OA = optic atrophy; OCT = optical coherence tomography; OPA1 = optic atrophy factor 1; PNP = peripheral neuropathy.

FIGURE 2 Evidence of Skin Sympathetic Denervation in *TH-Opa1*$^{+/-}$ Mice

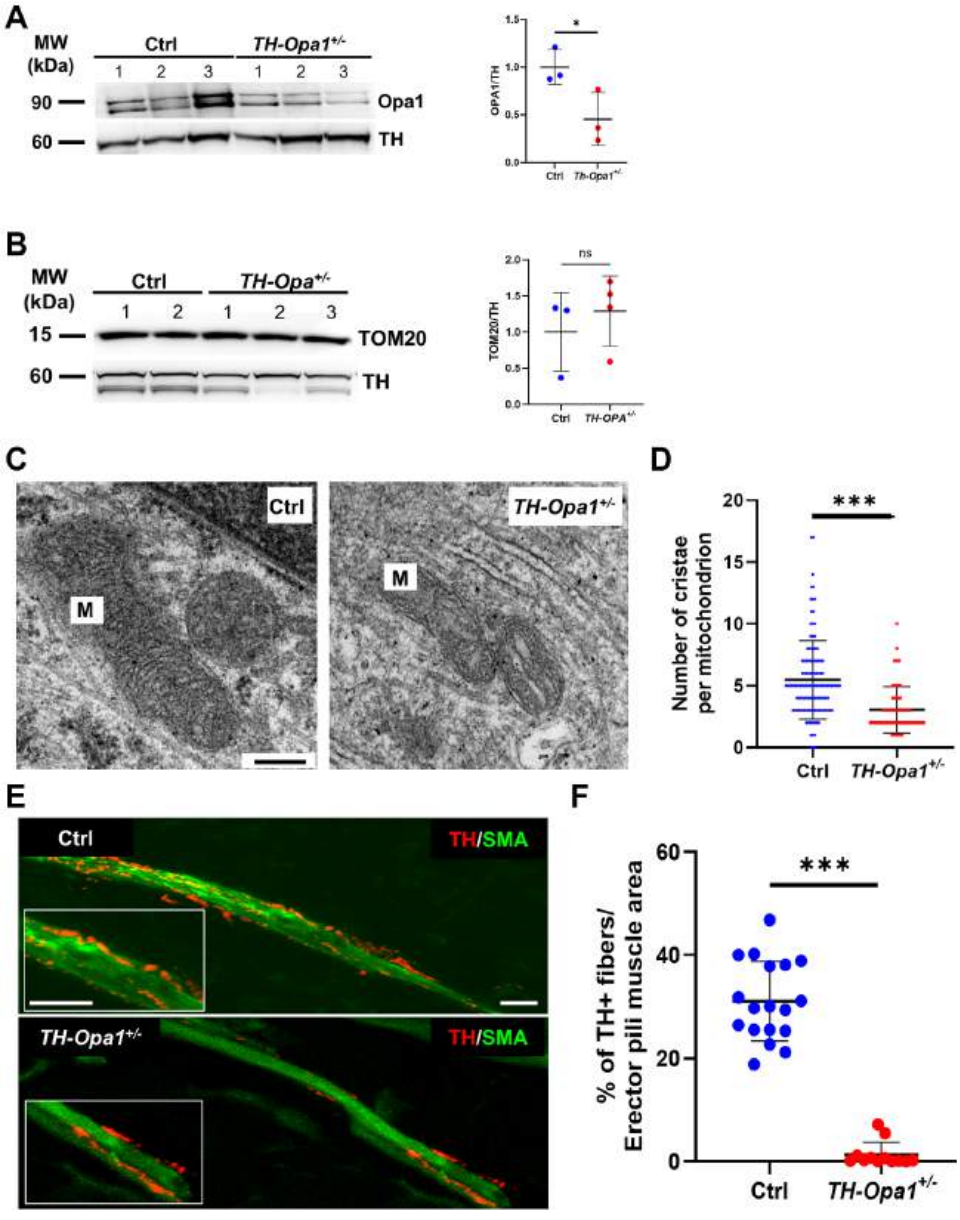

(A) Western blotting on protein extracts from superior cervical and stellate ganglia of adult control and *TH-Opa1*$^{+/-}$ male mice. TH ensured equal loading. Right panel: densitometry. Bars: SD. Differences by unpaired Student's *t*-test (each value is the pool of 4 ganglia from n = 6 control vs n = 6 *TH-Opa1*$^{+/-}$ mice). (B) Western blotting on protein extracts from superior cervical and stellate ganglia of adult control and *TH-Opa1*$^{+/-}$ male mice. TH ensured equal loading. Representative samples are shown. Right panel: densitometry. Differences between groups were determined using an unpaired Student's *t*-test (each value is the pool of 4 ganglia from n = 6 control vs n = 6 *TH-Opa1*$^{+/-}$ mice). (C) Transmission electron microscopy of stellate ganglia sections. Scale bar: 200 nm. (D) Quantification of cristae number per mitochondrion. Differences between groups were determined using Mann–Whitney U test (n = 120 control vs n = 53 TH-*Opa1*$^{+/-}$ mitochondria from 6 mice/group). (E) Confocal immunofluorescence on skin sections from adult control and *TH-Opa1*$^{+/-}$ mice, stained for TH and smooth muscle actin (SMA). Scale bar: 10 μm. The bottom-left panel represents a higher-magnification showing fragmentation of sympathetic fibers. Scale bar: 10 mm. (F) Quantification of sympathetic innervation density. Differences between groups were determined using Mann–Whitney U test (values from 3 images/section, 18 sections from 4 control mice vs 12 sections from 4 *TH-Opa1*$^{+/-}$ mice). Bars represent mean ± SD. **P* < 0.05, ****P* < 0.001. Ctrl = control; M = mitochondria; MW = molecular weight; ns = not significant; TOM20 = translocase of the outer membrane 20; other abbreviations as in Figure 1.

sympathetic neurodegeneration—characterized by fiber fragmentation and progressive loss of cardiac innervation—an effect that exceeds physiological aging alone.

REGIONAL REMODELING OF CARDIAC SYMPATHETIC INNERVATION WITH AGING. Given the elevated PVC burden and global sympathetic loss in *TH-Opa1*$^{+/-}$ hearts, we next assessed whether regional SN distribution was altered, specifically in the Epi and Endo layers of the left ventricle, in which the physiological innervation gradient contributes to the balanced effects of SN activation on electrophysiology.[34,36] The transmural gradient is preserved with aging, as age-related denervation occurs uniformly across both layers (SN density decrease: Epi: 22.65% ± 7.39%, $P < 0.001$; Endo: 20.29% ± 11.36%, $P < 0.001$) (Figure 5A). In contrast, 6-month-old *TH-Opa1*$^{+/-}$ mice exhibited a marked reduction in SN density in both layers (Epi: −60.07% ± 1.49%, $P < 0.001$; Endo: −56.60% ± 1.65%, $P < 0.001$). Despite this overall loss, the Epi/Endo SN density ratio remained comparable to controls (*TH-Opa1*$^{+/-}$: 1.93 ± 0.09 vs control: 2.09 ± 0.13; $P = 0.15$). However, in aged *TH-Opa1*$^{+/-}$ mice, SN loss became regionally unbalanced. The Endo region exhibited significantly greater degeneration than the Epi (SN density decrease: Epi: -32.21% ± 4.77%, $P < 0.001$; Endo: -50.36% ± 4.73%, $P < 0.001$), resulting in a significantly altered transmural SN density gradient (*TH-Opa1*$^{+/-}$: 2.69 ± 0.33 vs control: 2.03 ± 0.22; $P = 0.015$) (Figure 5A). To better characterize the impact of *Opa1* haploinsufficiency on SN architecture, we performed 3-dimensional reconstructions of SN arborization in clarified, whole-mounted myocardial blocks using 2-photon microscopy and TH immunostaining (Figures 5B and 5C, Supplemental Figures 4 to 6). These high-resolution reconstructions revealed pronounced rarefaction of SN processes in *TH-Opa1*$^{+/-}$ hearts, evidenced by reduced linear and neuronal density (total neuronal process length and total neuronal number of processes per tissue volume, respectively; linear density: Epi: Ctrl: $17.43 \times 10^{-4} \pm 5.11 \times 10^{-4}$ vs *TH-Opa1*$^{+/-}$: $6.97 \times 10^{-4} \pm 0.58 \times 10^{-4}$, $P = 0.008$; Endo: Ctrl: $7.20 \times 10^{-4} \pm 3.11 \times 10^{-4}$ vs *TH-Opa1*$^{+/-}$: $3.16 \times 10^{-4} \pm 0.59 \times 10^{-4}$, $P = 0.047$; neuronal density: Epi: Ctrl: $13.14 \times 10^{-6} \pm 2.65 \times 10^{-6}$ vs *TH-Opa1*$^{+/-}$: $4.93 \times 10^{-6} \pm 0.68 \times 10^{-6}$, $P = 0.002$; Endo: Ctrl: $5.08 \times 10^{-6} \pm 2.47 \times 10^{-6}$ vs *TH-Opa1*$^{+/-}$: $1.57 \times 10^{-6} \pm 0.22 \times 10^{-6}$, $P = 0.017$) (Figure 5D, Supplemental Figure 6A), and an almost complete loss of distal arborizations (third-order branches and beyond, Epi: I: Ctrl: 43.67 ± 11.24 vs *TH-Opa1*$^{+/-}$: 61.25 ± 0.95, $P = 0.023$, II: Ctrl: 23.67 ± 3.51 vs *TH-Opa1*$^{+/-}$: 26.00 ± 3.26, $P = 0.41$, III: Ctrl:

FIGURE 3 Impaired Neurogenic Control of Heart Function in *TH-Opa1*$^{+/-}$ Mice

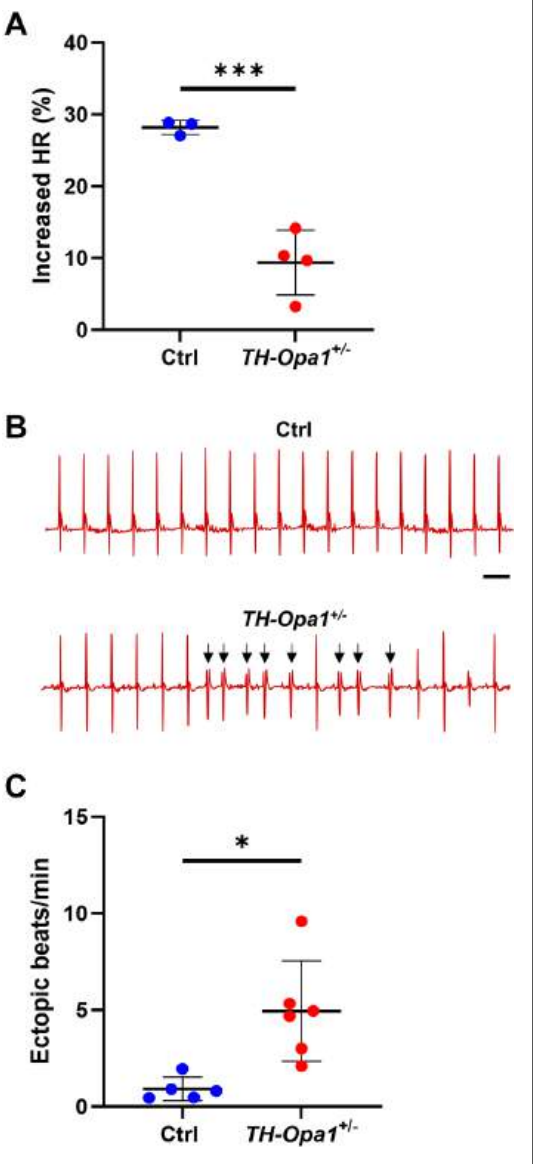

(A) Evaluation of the fractional heart rate (HR) increase 5 minutes after atropine administration, calculated as $(HR_{atropine} - HR_{basal})/HR_{atropine} \times 100$. Differences between groups were determined using an unpaired Student's *t*-test. (n = 3 control vs n = 4 *TH-Opa1*$^{+/-}$ adult mice). (B) Representative electrocardiogram (ECG) trace of adult control and *TH-Opa1*$^{+/-}$ mice. Black arrows evidence ectopic beats. Scale Bar: 100 msec. Arrows indicate ectopic beats. (C) Evaluation of the number of ectopic beats per minute in adult control and *TH-Opa1*$^{+/-}$ mice, calculated as the average over standardized 10-minute ECG recordings under resting conditions. Differences between groups were determined using an unpaired Student's *t*-test with Welch's correction (n = 5 control vs n = 6 *TH-Opa1*$^{+/-}$ mice). Bars represent mean ± SD. *$P < 0.05$, ***$P < 0.001$. Abbreviations as in Figures 1 and 2.

FIGURE 4 Cardiac Sympathetic Denervation in *TH-Opa1*$^{+/-}$ Mice

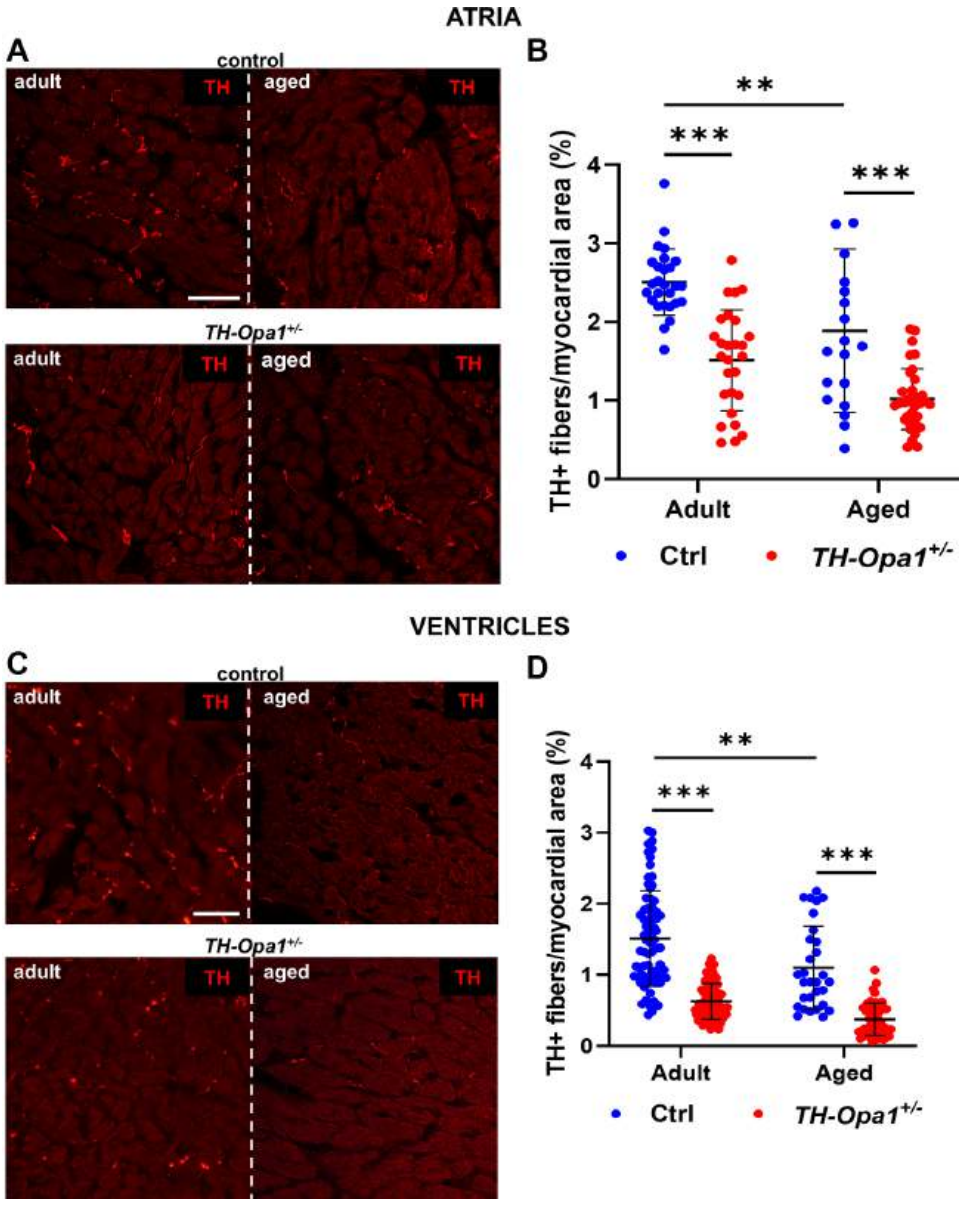

(A) Confocal images of right atrial sections from adult and aged control and *TH-Opa1*$^{+/-}$ male mice stained for TH. Scale bar: 50 μm. (B) Quantification of atrial sympathetic innervation (% area occupied by TH-positive fibers). Groups were compared using 2-way analysis of variance (ANOVA) with Tukey's post hoc test (6 months: n = 27 fields from 4 mice/group; 24 months: n = 18 fields from 3 control mice vs n = 33 fields from 5 *TH-Opa1*$^{+/-}$ mice). (C) Confocal images of left ventricular sections stained for TH. Scale bar: 50 μm. (D) Quantification of sympathetic innervation in the left ventricle as in (B). Groups were compared using 2-way ANOVA with Tukey's post hoc test (6 months: 73 Ctrl vs 79 *TH-Opa1*$^{+}$ fields from 5 mice/group; 24 months: 31 Ctrl vs 47 *TH-Opa1*$^{+/-}$ fields from 4 control vs 5 *TH-Opa1*$^{+/-}$ mice). Bars represent mean ± SD. $^{**}P < 0.01$, $^{***}P < 0.001$. Abbreviations as in Figures 1 and 2.

FIGURE 5 **Three-Dimensional Reconstruction of Cardiac Sympathetic Innervation in *TH-Opa1*$^{+/-}$ Mice**

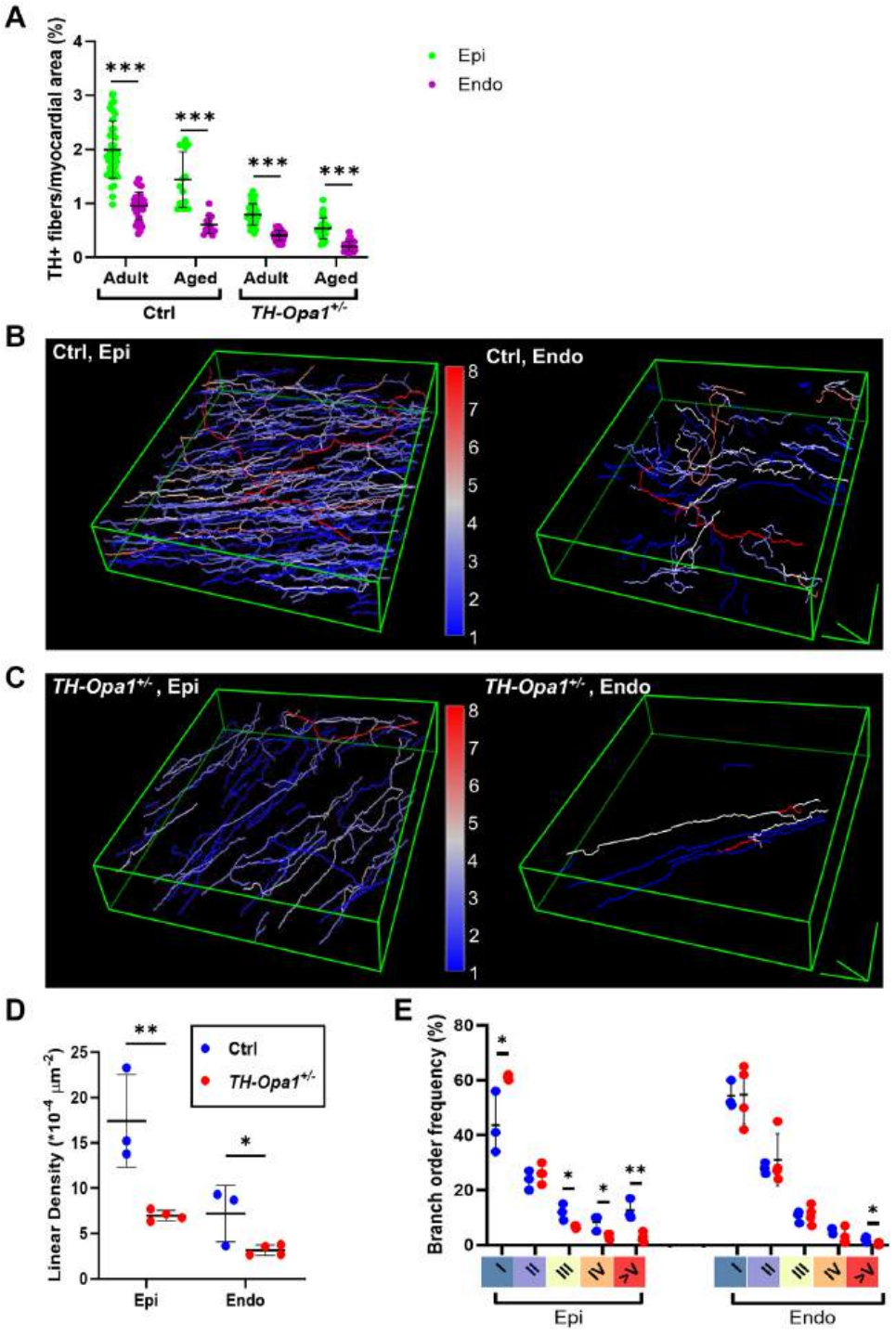

(A) Quantification of TH-positive sympathetic fiber density (% myocardial area) in sub-epicardial (Epi) and sub-endocardial (Endo) regions of the left ventricle in adult and aged control vs *TH-Opa1*$^{+/-}$ mice (n = 4 mice/group). (B and C) Representative 3-dimensional reconstructions of sympathetic networks (450 × 450 × 300 μm) in Epi and Endo regions from aged control and *TH-Opa1*$^{+/-}$ hearts, clarified and stained with anti-TH, imaged by custom 2-photon microscopy. Color code indicates branch order. (D) Quantification of neuronal linear density and (E) branch order frequency (n = 3 control vs n = 4 *TH-Opa1*$^{+/-}$ hearts). Groups were compared using 2-way ANOVA with Tukey's post hoc test. Bars represent mean ± SD. *$P < 0.05$, **$P < 0.01$, ***$P < 0.001$. Abbreviations as in Figures 1, 2, and 4.

12.00 ± 3.00 vs *TH-Opa1*$^{+/-}$: 6.75 ± 0.50, $P = 0.016$, IV: Ctrl: 8.33 ± 2.89 vs *TH-Opa1*$^{+/-}$: 3.25 ± 0.96, $P = 0.019$, > V: Ctrl: 12.67 ± 3.79 vs *TH-Opa1*$^{+/-}$: 2.75 ± 1.71, $P = 0.005$; Endo: I: Ctrl: 54.33 ± 4.94 vs *TH-Opa1*$^{+/-}$: 54.75 ± 10.69, $P = 0.95$, II: Ctrl: 82.00 ± 2.00 vs *TH-Opa1*$^{+/-}$: 31.00 ± 9.49, $P = 0.062$, III: Ctrl: 10.34 ± 2.08 vs *TH-Opa1*$^{+/-}$: 11.00 ± 3.38, $P = 0.77$, IV: Ctrl: 5.33 ± 1.16 vs *TH-Opa1*$^{+/-}$: 3.00 ± 2.89, $P = 0.24$, >V: Ctrl: 2.00 ± 1.00 vs *TH-Opa1*$^{+/-}$: 0.25 ± 0.50, $P = 0.027$) (Figure 5E). Notably, the Endo region in *TH-Opa1*$^{+/-}$ hearts was nearly devoid of innervation (Figure 5C, right panel), consistent with thin-section analyses. Furthermore, the number of fiber bundles extending from the epicardial surface into the myocardium was reduced in *Opa1* haploinsufficient hearts (Supplemental Figure 6B) (Ctrl: 24.60 ± 7.42 vs *TH-Opa1*$^{+/-}$: 3.84 ± 4.48, $P = 0.006$). In summary, high-resolution mapping of cSN demonstrates that *Opa1* haploinsufficiency – particularly in the context of aging – leads to severe and regionally unbalanced denervation, with near-complete loss of Endo innervation. This shift in the Epi/Endo SN density gradient likely contributes to the impaired chronotropic response to atropine and the elevated PVCs incidence observed in *TH-Opa1*$^{+/-}$ mice.

IMPAIRED NGF UPTAKE AND REDUCED NEUROTROPHIC SIGNALING IN OPA1-DEFICIENT NEURONS. The differentiation, arborization, and survival of cSN critically depend on adequate neurotrophic support from myocardial-derived NGF. NGF signals through its high- and low-affinity receptors, TrkA and p75, respectively, and is retrogradely transported to the soma as ligand-receptor complex.[37-39] This process relies on intact mitochondrial function and proper intracellular transport, which require organelle positioning and cytoskeletal dynamics.[40-42] Building on the observed SN degeneration and altered innervation gradients, we hypothesized that impaired neurotrophic support, particularly NGF/TrkA signaling, might underlie the vulnerability of cSN in *TH-Opa1*$^{+/-}$ mice. In *TH-Opa1*$^{+/-}$ mice, SN soma appeared atrophic, and NGF immunoreactivity was markedly reduced (Figures 6A and 6B) (Ctrl: 8.05 ± 2.70 vs *TH-Opa1*$^{+/-}$: 5.83 ± 2.63, $P < 0.001$). Western blot analysis confirmed decreased levels of mature NGF (Ctrl: 1.24 ± 0.42 vs *TH-Opa1*$^{+/-}$: 0.45 ± 0.05; $P = 0.009$) and a lower NGF/pro-NGF ratio (Ctrl: 0.99 ± 0.39 vs *TH-Opa1*$^{+/-}$: 0.50 ± 0.11; $P = 0.058$), alongside reduced phosphorylation of the downstream NGF effector protein kinase B (phosphorylated AKT/total AKT: Ctrl: 0.79 ± 0.09 vs *TH-Opa1*$^{+/-}$: 0.40 ± 0.07, $P = 0.004$; phosphorylated AKT/TH: Ctrl: 1.18 ± 0.08 vs *TH-Opa1*$^{+/-}$: 0.37 ± 0.12, $P < 0.001$; total AKT/TH: Ctrl: 1.52 ± 0.29 vs *TH-Opa1*$^{+/-}$: 0.92 ± 0.30, $P = 0.10$) (Figures 6C and 6D). These changes were not due to altered expression of NGF receptors (*TrkA*: Ctrl: 1.00 ± 0.47 vs *TH-Opa1*$^{+/-}$: 1.07 ± 0.38, $P = 0.85$, *p75*: Ctrl: 1.00 ± 0.25 vs *TH-Opa1*$^{+/-}$: 1.04 ± 0.22, $P = 0.86$, *TrkA/p75*: Ctrl: 1.00 ± 0.71 vs *TH-Opa1*$^{+/-}$: 0.92 ± 0.16, $P = 0.85$) in cSN or to reduced cardiac NGF availability (Ctrl: 0.26 ± 0.22 vs *TH-Opa1*$^{+/-}$: 0.26 ± 0.10; $P = 0.96$), both of which remained unchanged (Figures 6E and 6F), suggesting a defect in NGF uptake, processing, or intracellular trafficking. To further explore this, we cultured primary cSN isolated from the superior cervical and stellate ganglia of *TH-Opa1*$^{+/-}$ mice and controls. In vitro, OPA1-deficient neurons recapitulated the in vivo phenotype, including altered mitochondrial morphology characterized by shortened branches (Ctrl: 10.58 ± 2.15 vs *TH-Opa1*$^{+/-}$: 9.49 ± 2.30; $P = 0.033$) (Figures 7A and 7B), without changes in mitochondrial number (Supplemental Figure 7) (Ctrl: 325.8 ± 90.39 vs *TH-Opa1*$^{+/-}$: 347.6 ± 121.3; $P = 0.37$). In addition, cultured *TH-Opa1*$^{+/-}$ SN exhibited soma atrophy, neurite shortening (Ctrl: 2,558 ± 1,191 vs *TH-Opa1*$^{+/-}$: 1,845 ± 936.2; $P < 0.001$), reduced axonal sprouting (Ctrl: 147.1 ± 85.40 vs *TH-Opa1*$^{+/-}$: 104.4 ± 56.79; $P < 0.001$), and decreased anti-NGF fluorescence intensity (Ctrl: 1,245 ± 349.4 vs *TH-Opa1*$^{+/-}$: 978.5 ± 341.1; $P = 0.004$) (Figures 7C to 7G). These results support the hypothesis that *Opa1* haploinsufficiency compromises retrograde NGF transport. To infer whether OPA1-deficient SNs are more dependent on exogenous NGF, we assayed neuronal survival in cultured primary SNs maintained at varying NGF concentrations (100, 25, and 0 ng/mL). At 100 ng/mL, *TH-Opa1*$^{+/-}$ SNs displayed similar cell density to controls despite morphological abnormalities (Ctrl: 1.00 ± 0.36 vs *TH-Opa1*$^{+/-}$: 0.87 ± 0.34; $P = 0.42$). However, reducing NGF to 25 ng/mL (well tolerated by control neurons) led to a sharp decline in the density of *TH-Opa1*$^{+/-}$ SNs, comparable to that seen in NGF-deprived conditions (Ctrl: 0.93 ± 0.36 vs *TH-Opa1*$^{+/-}$: 0.56 ± 0.24; $P = 0.022$) (Figures 7H and 7I). Together, these data indicate that *Opa1* haploinsufficiency impairs neurotrophic efficiency, likely through defective NGF uptake and transport.

DISRUPTED MITOCHONDRIAL DYNAMICS UNDERLIE IMPAIRED NGF TRAFFICKING IN OPA1-DEFICIENT NEURONS AND ARE RESCUED BY *DRP1* SILENCING. To dissect the molecular mechanisms linking *Opa1* haploinsufficiency to SN degeneration, we used neuronally differentiated PC12 cells transduced with a viral vector encoding a short hairpin RNA targeting *Opa1* (sh*Opa1*). The viral load was titrated to reduce

FIGURE 6 Impaired NGF Signaling in Sympathetic Ganglia From *TH-Opa1*$^{+/-}$ Mice

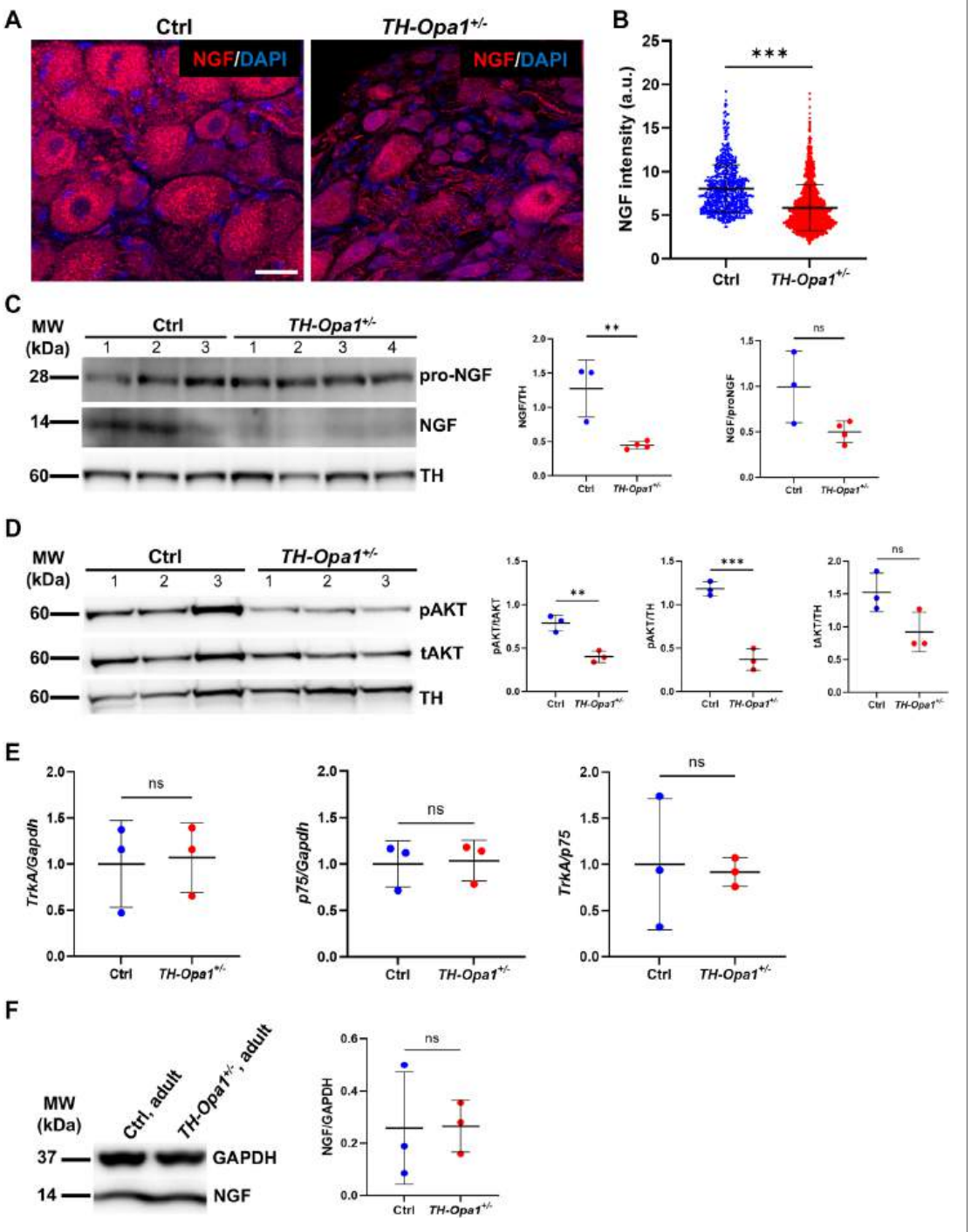

(A) Confocal images of stellate ganglia sections from control and *TH-Opa1*$^{+/-}$ mice stained for nerve growth factor (NGF) and 4',6-diamidino-2-phenylindole. Scale bar: 50 μm. (B) NGF fluorescence intensity in neuronal somas (n = 619 somas from 3 control mice vs n = 2265 somas from 4 *TH-Opa1*$^{+/-}$ mice). (C and D) Western blot on pooled extracts from superior cervical and stellate ganglia. TH was used as loading control (each lane corresponds to 4 pooled ganglia; a total of 12 ganglia from 6 control vs 16 ganglia from 8 *TH-Opa1*$^{+/-}$ mice were analyzed). (E) Quantitative reverse transcription polymerase chain reaction on ganglia extracts (each point = 4 ganglia; n = 12 ganglia from 6 control vs n=16 ganglia from *8 TH-Opa1*$^{+/-}$ mice). (F) Representative Western blot on heart protein extracts. Glyceraldehyde 3-phosphate dehydrogenase (GAPDH) was used as loading control. Right panel: densitometry. Each lane corresponds to 2 pooled hearts; n = 6 control vs n = 6 *TH-Opa1*$^{+/-}$ mice. Differences between groups were determined using an unpaired Student's *t*-test. Bars represent mean ± SD. $^{**}P < 0.01$, $^{***}P < 0.001$. AKT = protein kinase B; pAKT = phosphorylated AKT; tAKT = total AKT; TrkA = tropomyosin receptor kinase A; other abbreviations as in Figures 1 and 2.

FIGURE 7 Morphological Alterations and Impaired NGF Signaling in Cultured *TH-Opa1*$^{+/-}$ SNs

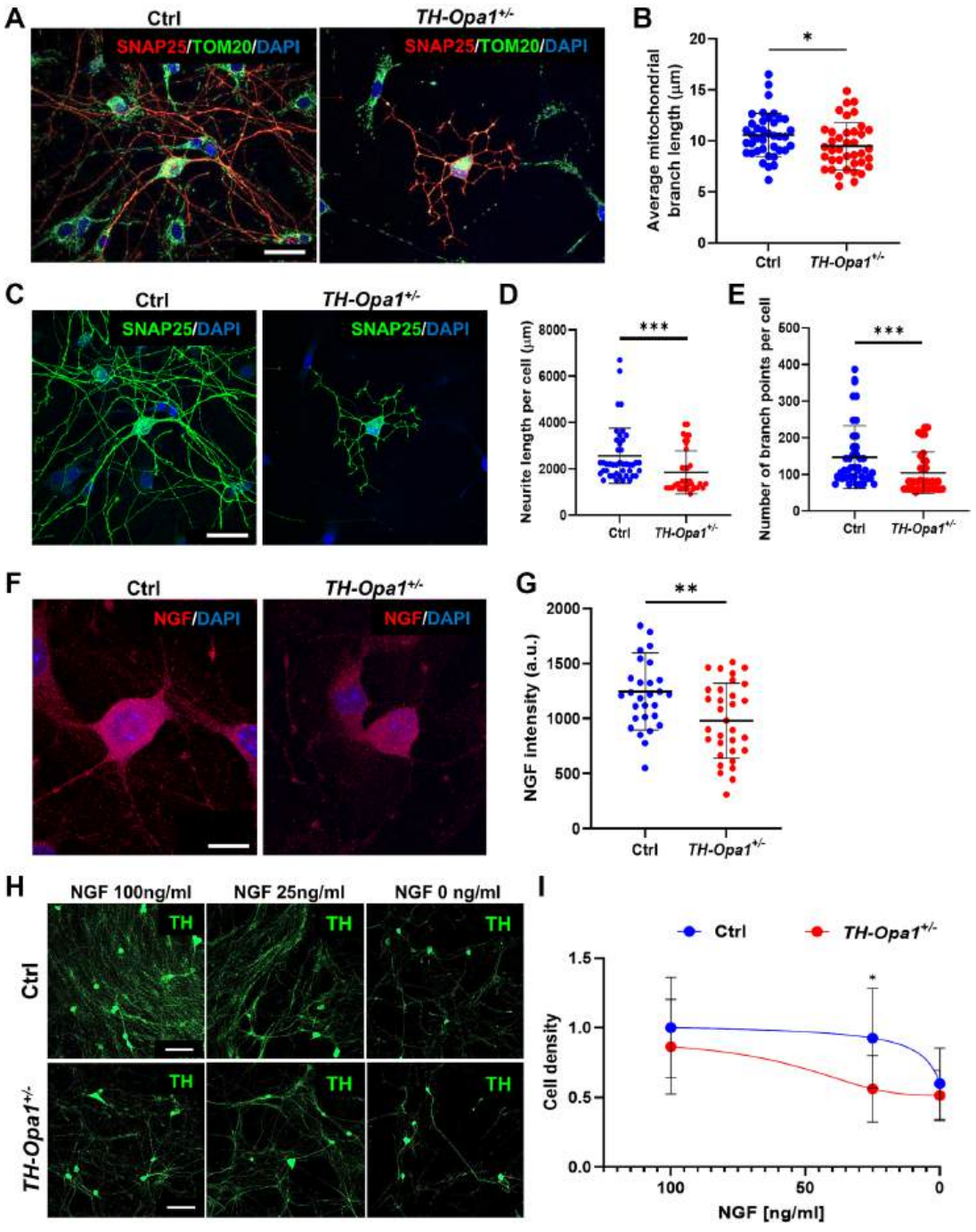

(A) Confocal images of primary sympathetic neurons (SNs) from control and *TH-Opa1*$^{+/-}$ mice, stained with anti-SNAP25, anti-TOM20, and 4′,6-diamidino-2-phenylindole (DAPI). Scale bar: 25 µm. (B) Quantification of mitochondrial branch length. Differences between groups were determined using unpaired Student's *t*-test (>12,314 branches from 39 SN/group, 3 mice each). (C) Confocal images of primary SNs from control and *TH-Opa1*$^{+/-}$ mice, stained with anti-SNAP25 and DAPI. Scale bar: 25 µm. (D) Neurite length and (E) branching quantification. Differences between groups were determined using Mann-Whitney U test (n = 43 control vs n = 39 *TH-Opa1*$^{+/-}$ SNs from 4 mice/group). (F) Confocal images of primary SNs from control and *TH-Opa1*$^{+/-}$ mice, stained with anti-NGF and DAPI. Scale bar: 10 µm. (G) NGF immunoreactivity in SN somas. Differences between groups were determined using an unpaired Student's *t*-test (n = 42 control vs n = 22 *TH-Opa1*$^{+/-}$ somas from 4 mice/group). (H) Confocal images of primary SNs from control and *TH-Opa1*$^{+/-}$ mice, cultured with different NGF concentrations, and stained with anti-TH and DAPI. Scale bar: 70 µm (I) SN density after NGF withdrawal. Differences between groups were determined using unpaired Student's *t*-test (mean of 6 replicates from 2 independent cultures). Bars represent mean ± SD. *$P < 0.05$, **$P < 0.01$, ***$P < 0.001$. SNAP25 = synaptosomal-associated protein, 25kDa; other abbreviations as in Figures 1, 2, and 6.

OPA1 protein levels, mimicking haploinsufficiency (Supplemental Figure 8A) (Ad-Empty: 1.00 ± 0.14 vs Ad-sh*Opa1*: 0.28 ± 0.06; $P = 0.001$). Consistent with the results obtained in sympathetic ganglia, the overall mitochondrial content was unchanged, as indicated by TOMM20 protein levels normalized to TH (Supplemental Figure 8A) (Ad-Empty: 1.00 ± 0.24 vs Ad-sh*Opa1*: 1.15 ± 0.17; $P = 0.41$). In contrast, mitochondrial morphology was markedly altered, with decreased branching (Ad-Empty: 443.40 ± 137.80 vs Ad-sh*Opa1*: 283.80 ± 84.50; $P < 0.001$), shorter branch length (Ad-Empty: 0.40 ± 1.64 vs Ad-sh*Opa1*: 4.87 ± 1.21; $P = 0.021$), and reduced membrane potential (Slope: Ad-Empty: 1.05 ± 0.08 vs Ad-sh*Opa1*: -0.12 ± 0.07, $P < 0.001$) (Supplemental Figures 8B to 8E). shOpa1-expressing PC12 cells phenocopied several key features observed in primary *TH-Opa1*$^{+/-}$ SN, including shorter (Ad-Empty: 269.10 ± 167.00 vs Ad-sh*Opa1*: 56.01 ± 39.07; $P < 0.001$) and less branched neurites (Ad-Empty: 7.24 ± 5.33 vs Ad-sh*Opa1*: 0.97 ± 0.95, $P < 0.001$), lower NGF content, as measured by both immunofluorescence in the cell soma (Ad-Empty: 22.29 ± 11.39 vs Ad-sh*Opa1*: 12.21 ± 6.59; $P = 0.002$) and Western blotting (Ad-Empty: 1.07 ± 0.23 vs Ad-sh*Opa1*: 0.39 ± 0.11; $P = 0.016$), and heightened sensitivity to NGF withdrawal, resulting in cell death upon milder deprivation (200 ng/mL: Ad-Empty: 0.86 ± 0.09 vs Ad-sh*Opa1*: 0.92 ± 0.27, $P = 0.98$; 100 ng/mL: Ad-Empty: 0.99 ± 0.20 vs Ad-sh*Opa1*: 0.89 ± 0.06, $P = 0.91$; 50 ng/mL: Ad-Empty: 1.00 ± 0.21 vs Ad-sh*Opa1*: 0.75 ± 0.16, $P = 0.005$; 10 ng/mL: Ad-Empty: 0.88 ± 0.12 vs Ad-sh*Opa1*: 0.39 ± 0.04, $P < 0.001$; 0 ng/mL: Ad-Empty: 0.42 ± 0.09 vs Ad-sh*Opa1*: 0.12 ± 0.04, $P = 0.021$) (**Figures 8A to 8E**, Supplemental Figures 9A to 9D). To mechanistically link these findings to defective neurotrophic support, we performed live-cell confocal imaging to track TrkA-positive vesicles and assess NGF/TrkA signalosome dynamics. In sh*Opa1*-expressing neurons, both anterograde (Ad-Empty: 40.85 ± 43.94 vs Ad-sh*Opa1*: 12.23 ± 11.34; $P = 0.012$) and retrograde (Ad-Empty: 18.71 ± 24.06 vs Ad-sh*Opa1*: 6.96 ± 6.59; $P = 0.005$) transport velocity of TrkA-associated vesicles were significantly reduced compared to control-transduced cells (**Figures 8F and 8G**), confirming a trafficking defect. To assess whether mitochondrial fragmentation contributes causally to these defects, we silenced *Drp1*, a key mediator of mitochondrial fission,[43,44] in sh*Opa1*-expressing SNs. *Drp1* knockdown significantly improved neurite length and branching (Ad-sh*Opa1* plus vehicle: 42.90 ± 40.20 vs Ad-sh*Opa1* plus si*Drp1*: 104.60 ± 88.11; $P <$ 0.001) (**Figures 8H and 8I**, Supplemental Figure 10), demonstrating that restoring mitochondrial network integrity can rescue the neuronal phenotype. Collectively, these results identify abnormal mitochondrial dynamics as a central driver of the neurotrophic deficit in OPA1-deficient SNs. OPA1 haploinsufficiency impairs NGF trafficking and signaling through disrupted mitochondrial morphology and transport, weakening pro-survival and differentiation pathways. Suppression of mitochondrial fission by *Drp1* silencing effectively restored neurite architecture and NGF responsiveness, pinpointing mitochondrial dynamics as both a mechanistic determinant and a tractable therapeutic target.

DISCUSSION

In this study, we demonstrate that OPA1 haploinsufficiency—the primary genetic mechanism underlying DOA—drives a previously unrecognized form of systemic sympathetic neurodegeneration. Using human skin biopsy specimens, transgenic mouse models, and cellular systems, we show that OPA1-deficient SNs undergo progressive structural and functional decline, resulting in both cardiac and peripheral sympathetic denervation. These findings provide a mechanistic explanation for the unresolved cardiovascular and autonomic symptoms seen in a subset of DOA patients, particularly those with multisystem involvement ("DOA-plus"). Importantly, we identify defective NGF/TrkA signaling and trafficking as a downstream consequence of mitochondrial dysfunction, expanding the pathophysiological spectrum of DOA beyond the optic nerve into the autonomic nervous system.

OPA1 is a mitochondrial inner membrane GTPase that governs multiple facets of mitochondrial biology, including inner membrane fusion, cristae architecture, mitochondrial DNA maintenance, and regulation of mitophagy and apoptosis.[29,45] Although DOA has classically been considered a retinal ganglion cell-specific disorder, its clinical spectrum frequently includes systemic features—sensorineural hearing loss,[26] myopathy,[32] ataxia,[14] and cardiomyopathy[5,21]—collectively defined under the DOA-plus variant definition.[8,9,13] Previous reports have attributed cardiac manifestations to cardiomyocyte-intrinsic defects in OPA1.[14-18] Our findings complement and extend these observations by uncovering neuron-specific, progressive degeneration of sympathetic fibers as an additional pathogenic mechanism. These findings identify the sympathetic nervous system as a new cellular target of OPA1 deficiency and suggest it may mediate the systemic manifestations of DOA.

FIGURE 8 OPA1 Deficiency Impairs NGF/TrkA Signaling and Neuronal Morphology in SNs Rescued by *Drp1* Silencing

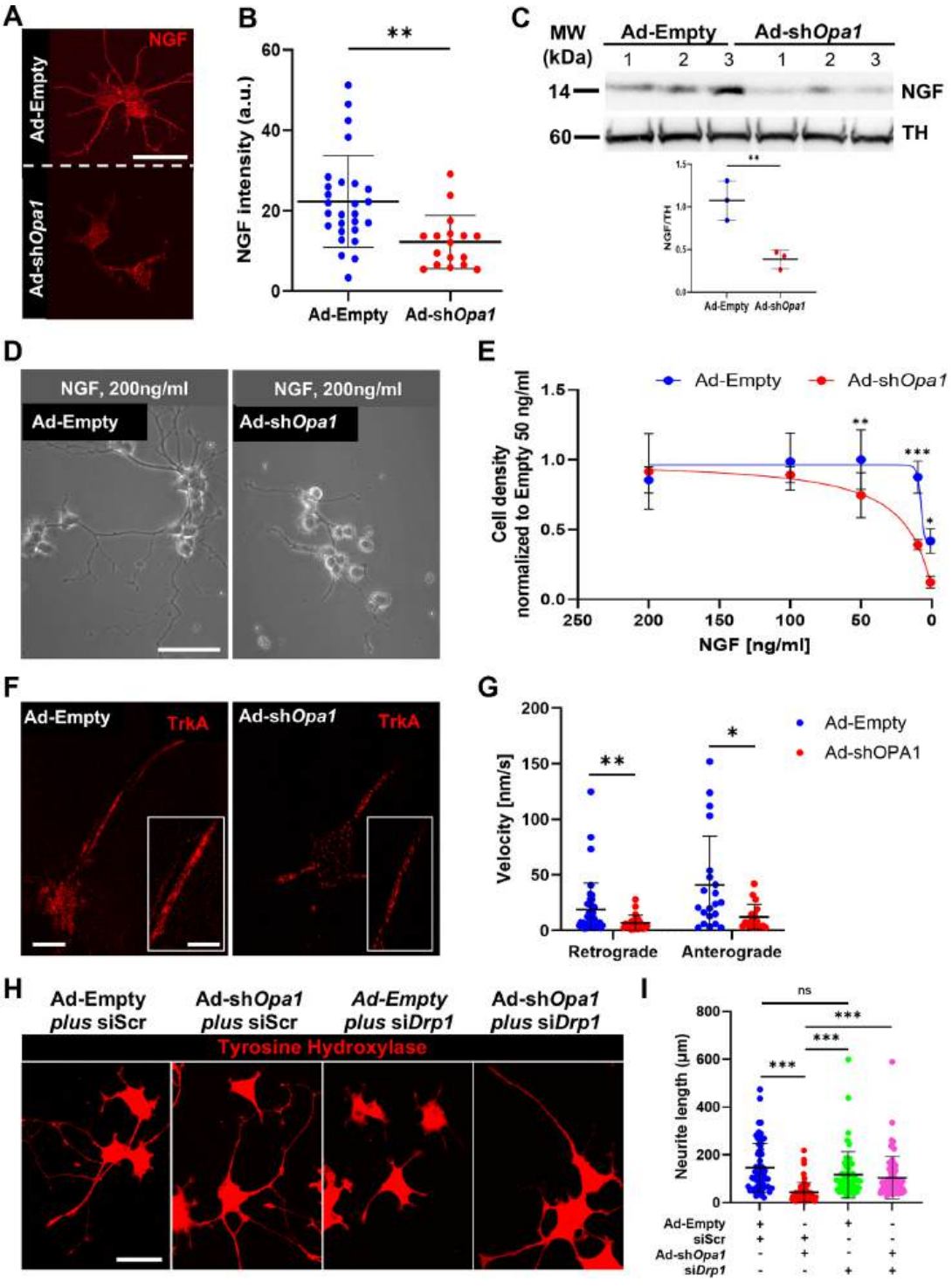

Continued on the next page

cSNs form specialized neurocardiac junctions with cardiomyocytes, enabling precise regulation of heart rate, contractility, and electrophysiological stability.[36,43,46,47] These neurons are regionally distributed across the myocardium in patterns that meet physiological requirements. It is well accepted that spatial denervation disrupts the regional balance of adrenergic tone, contributing to electrophysiological instability.[36,43,46,47] In our TH-specific *Opa1* haploinsufficient mouse model, we observed progressive and regionally patterned cardiac denervation, culminating in near-complete sympathetic fiber loss in aged animals. Early degeneration was more prominent in regions with initially dense innervation, suggesting a "use-vulnerability" paradigm. This pattern was recapitulated in peripheral tissues: both human and murine skin biopsy specimens revealed marked loss of cutaneous sympathetic fibers, confirming the systemic nature of the neuropathy and establishing SNs as direct targets of OPA1-related degeneration.

Mechanistically, we identify disruption of NGF/TrkA signaling as a central consequence of OPA1 deficiency. Although NGF production (from the myocardium) and TrkA receptor expression (in SNs) were preserved, OPA1-deficient SNs displayed impaired retrograde transport of NGF/TrkA endosomes, leading to reduced activation of downstream pro-survival pathways, including protein kinase B phosphorylation. NGF signalosome trafficking is an energy-intensive process that depends on mitochondrial integrity and axonal bioenergetics. Consistent with this, overall mitochondrial content remained unchanged in sympathetic ganglia and PC12 neurons, whereas ultrastructural and functional analyses revealed severe defects in cristae morphology, network branching, and membrane potential. The results indicate a pathogenic mechanism driven by dysfunction and quality defects, rather than loss of mitochondria. Although adenosine triphosphate levels were not directly quantified, it is plausible that OPA1-related defects in mitochondrial dynamics and positioning compromise axonal energy supply, thereby disrupting neurotrophic signaling. In this model, defective mitochondrial fusion impairs trophic support and triggers a degenerative cascade. Suppression of mitochondrial fission through *Drp1* silencing restored neurite architecture in OPA1-deficient neurons. These results indicate that altered mitochondrial dynamics are not merely a consequence but also a driver of neuronal degeneration and highlight mitochondrial fusion-fission balance as a potential therapeutic target.

The neurocardiac axis functions as a bidirectional feedback system: cardiomyocytes provide essential support to SNs, whereas sympathetic input maintains myocardial electrophysiological homeostasis.[36,46-50] In the setting of systemic OPA1 deficiency, this reciprocity becomes maladaptive—impaired cardiomyocyte support exacerbates neuronal vulnerability, whereas sympathetic denervation destabilizes cardiac function, creating a vicious cycle of neurocardiac degeneration. Therefore, our findings reposition DOA within the broader class of mitochondrial neurodegenerative disorders characterized by defects in mitochondrial dynamics, axonal transport, and neurotrophic signaling. SNs, with their exceptionally long axons and high metabolic demands, appear particularly susceptible to these perturbations. Analogous mechanisms have been implicated in Alzheimer's,[50-52] Parkinson's,[53,54] and Huntington's disease[55,56] and amyotrophic lateral sclerosis,[57,58] all of which feature impaired axonal transport and defective neurotrophic signaling as early pathological events.[59-66] Our data highlight shared vulnerabilities across mitochondrial neuropathies and identify the NGF/TrkA axis as a unifying target for intervention.

FIGURE 8 Continued

(A) Immunofluorescence of NGF in Ad-Empty vs Ad-sh*Opa1* SNs. Scale bar: 40 μm. (B) Soma NGF intensity. Differences between groups were determined using Mann–Whitney U test (n = 27 Ad-Empty vs n = 17 Ad-sh*Opa1* cells from 3 independent experiments). (C) Western blot and densitometry. TH was used as loading control. Differences between groups were determined using an unpaired Student's *t*-test (each data point represents a pool of 2 wells; n = 6 total replicates from n = 3 independent experiments). (D and E) SN density after NGF withdrawal. Groups were compared using 2-way ANOVA with Sidak's post hoc test (n = 6 replicates from 2 independent experiments). Panels in (D) are representative of cells treated with 200 ng/mL NGF. (F) Images of Ad-Empty and Ad-shOpa1 cells expressing TrkA-dsRed. Scale bar: 10 mm (low magnification); 5 mm (high magnification). (G) TrkA-dsRed velocity. Differences between groups were determined using Mann–Whitney U test (20 cells/group). (H) Confocal immunofluorescence in Ad-Empty vs Ad-shOpa1 cells with or without *Drp1* silencing. Cells were stained with anti-TH and DAPI. (I) Quantification of neurite length in the same experimental group of (H). Groups were compared using Brown-Forsythe ANOVA test with Dunnett's post hoc test (Ad-Empty: n = 61 cells; Ad-sh*Opa1*: n = 64 cells; Ad-Empty plus si*Drp1*: n = 61 cells; Ad-sh*Opa1* plus si*Drp1*: n = 67 cells. Three independent experiments). Bars represent mean ± SD. *$P < 0.05$, **$P < 0.01$, ***$P < 0.001$. Ad = adenoviral vector; dsRed = red fluorescent protein; sh = short hairpin RNA; siDrp1 = small interfering RNA targeting Drp1; siScr = small interfering RNA scramble; other abbreviations as in **Figures 1, 2, 4, 6, and 7**.

From a translational perspective, our results carry several implications. First, they suggest that skin biopsy—a minimally invasive, clinically accessible tissue—could serve as a diagnostic window into sympathetic neurodegeneration in DOA and other mitochondrial diseases. Second, our in vitro experiments showed that high NGF concentrations partially restored neuronal integrity in OPA1-deficient SNs, supporting the concept that enhancing neurotrophic tone may counteract mitochondrial dysfunction and delay degeneration. Although systemic NGF delivery remains impractical because of limited tissue specificity and off-target effects, these findings provide proof-of-principle for strategies aimed at restoring neurotrophic signaling, such as targeted NGF delivery, small-molecule TrkA agonists, or pharmacologic modulators of mitochondrial dynamics.

The SN-specific haploinsufficient mouse model allowed us to isolate the neuron-autonomous contribution of OPA1 to sympathetic degeneration. Although patients carry systemic *OPA1* mutations affecting all tissues, this targeted model dissected the neuronal component in the absence of non-neuronal confounders. This approach directly demonstrated SN vulnerability and established a causal link between neuronal OPA1 loss and sympathetic denervation. Nonetheless, the full clinical spectrum of DOA likely reflects additional reciprocal interactions between cardiomyocytes and SNs, which remain to be explored in systemic OPA1 deficiency models. Moreover, heterogeneity among *OPA1* variants and variable penetrance may shape the severity of autonomic involvement. Future studies should characterize the temporal evolution of sympathetic loss in patients and determine whether circulating biomarkers or imaging approaches (eg, meta-ioidobenzylguanidine scintigraphy) can detect early autonomic dysfunction. Testing combinatorial therapies that support both mitochondrial function and neurotrophic signaling in vivo will be crucial to translate these findings into effective clinical interventions.

STUDY LIMITATIONS. Although the SN-specific *Opa1* haploinsufficient mouse model enabled us to pinpoint the neuronal contribution to sympathetic neurodegeneration, it was not intended to reproduce the full multisystem complexity seen in DOA, where numerous cell types and tissues are affected. In addition, the bidirectional interaction between SNs and cardiomyocytes, which is critical for cardiac homeostasis, remains to be examined in models with systemic OPA1 deficiency. We also did not investigate the parasympathetic nervous system, which may contribute to the autonomic phenotype. Finally, future clinical studies should clarify the time course of SN loss and assess whether early autonomic dysfunction can be detected with circulating biomarkers or advanced imaging techniques. Both male and female mice were evaluated in our study and showed comparable phenotypes; however, only male data are shown for clarity and consistency.

CONCLUSIONS

We redefine DOA as a systemic mitochondrial disorder characterized by early and progressive degeneration of the sympathetic nervous system. We uncover a pathogenic mechanism whereby OPA1 haploinsufficiency disrupts NGF/TrkA trafficking and signaling, conferring selective vulnerability to SNs and promoting cardiac dysfunction. These insights clarify the multisystem nature of DOA, provide mechanistic grounding for its autonomic manifestations, and identify the SN as a rational and actionable therapeutic target. By linking mitochondrial integrity to neurotrophic signaling, this work establishes a framework for mechanism-based interventions aimed at preserving autonomic and cardiac function in mitochondrial disease.

ACKNOWLEDGMENTS The authors thank Drs Arianna Scalco, Nicola Pianca, Martina Semenzato, and Mauro Franzoso for initial technical support, and Dr Patrizia Rosa for providing PC12 cells; Dr Leonardo Caporali for *OPA1* sequencing and diagnosis of all patients enrolled in the study; and the late Mr Gilberto Benetton for supporting Mongillo's laboratory.

FUNDING SUPPORT AND AUTHOR DISCLOSURES

Supported by the University of Padova (SID-2022 to Dr Mongillo and Stars grant "SKoP" to Dr Zaglia.), and PRIN-20229PX74A to Dr Zaglia. Further support to this work comes from the "Ricerca Corrente" funding from the Italian Ministry of Health and from the #NEXT-GENERATIONEU (NGEU) funded by the Ministry of University and Research (MUR), National Recovery and Resilience Plan (NRRP), project MNESYS (PE0000006) - A Multiscale integrated approach to the study of the nervous system in health and disease (DN. 1553 11.10.2022) to Dr Carelli, Dr La Morgia, Dr Donadio, and Dr Liguori. All other authors have reported that they have no relationships relevant to the contents of this paper to disclose.

ADDRESS FOR CORRESPONDENCE: Dr Tania Zaglia, Department of Biomedical Sciences, University of Padova, Via Ugo Bassi 58/B, 35122 Padova, Italy. E-mail: tania.zaglia@unipd.it.

PERSPECTIVES

COMPETENCY IN MEDICAL KNOWLEDGE: Our findings highlight the critical role of OPA1 in maintaining peripheral SN integrity and function. *OPA1* haploinsufficiency markedly reduces cutaneous and cardiac sympathetic-fiber density and induces morphological abnormalities, findings replicated both in DOA patients and in *TH-Opa1*$^{+/-}$ mice. This denervation is accompanied by a blunted chronotropic response after parasympathetic blockade and a higher incidence of ventricular arrhythmias, underscoring the contribution of sympathetic dysfunction to cardiovascular risk. Mechanistically, OPA1 deficiency impairs the retrograde transport of NGF and attenuates NGF/TrkA signaling; combined with mitochondrial dysfunction, these changes render sympathetic fibers prone to atrophy and degeneration. Quantifying peripheral sympathetic innervation - e.g. *via* skin biopsy - may therefore provide an early diagnostic and risk-stratification tool for mitochondrial neurocardiac disorders.

TRANSLATIONAL OUTLOOK: The *TH-Opa1*$^{+/-}$ mouse and *Opa1*-silenced PC12 cells provide robust pre-clinical platforms for dissecting sympathetic neurodegeneration and testing neuroprotective therapies. Their documented deficits in NGF/TrkA retrograde transport and mitochondrial dynamics point toward interventions that restore mitochondrial function or enhance neurotrophic trafficking. The detailed mapping of regional cardiac sympathetic denervation, characterized by selective subendocardial fiber loss, supports the development of pharmacologic or neuro-modulatory treatments tailored to the spatial pattern and extent of innervation defects. In parallel, skin biopsy offers a minimally invasive tool for diagnosis, risk stratification, and longitudinal monitoring in future trials. Collectively, these advances call for a coordinated effort across neurology, cardiology, and mitochondrial biology to improve management of neurodegenerative disorders with cardiac involvement. In line with recent perspectives on neuro-cardiac cross-talk,[47–49] our findings emphasize the therapeutic potential of targeting autonomic dysfunction - through strategies that reinforce NGF/TrkA signaling and mitochondrial integrity - to improve cardiovascular outcomes in mitochondrial disease.

REFERENCES

1. Cipolat S, De Brito OM, Dal Zilio B, Scorrano L. OPA1 requires mitofusin 1 to promote mitochondrial fusion. *Proc Natl Acad Sci U S A*. 2004;101:15927.

2. Alexander C, Votruba M, Pesch UEA, et al. OPA1, encoding a dynamin-related GTPase, is mutated in autosomal dominant optic atrophy linked to chromosome 3q28. *Nat Genet*. 2000;26:211–215.

3. Nasca A, Rizza T, Doimo M, et al. Not only dominant, not only optic atrophy: expanding the clinical spectrum associated with OPA1 mutations. *Orphanet J Rare Dis*. 2017;12:1–10.

4. Spiegel R, Saada A, Flannery PJ, et al. Fatal infantile mitochondrial encephalomyopathy, hypertrophic cardiomyopathy and optic atrophy associated with a homozygous OPA1 mutation. *J Med Genet*. 2016;53:127–131.

5. Chen L, Liu T, Tran A, et al. OPA1 mutation and late-onset cardiomyopathy: mitochondrial dysfunction and mtDNA instability. *J Am Heart Assoc*. 2012;1:e003012.

6. Carelli V, Sabatelli M, Carrozzo R, et al. "Behr syndrome" with OPA1 compound heterozygote mutations. *Brain*. 2015;138:e321.

7. Pretegiani E, Rufa A, Gallus GN, Cardaioli E, Malandrini A, Federico A. Spastic paraplegia in 'dominant optic atrophy plus' phenotype due to OPA1 mutation. *Brain*. 2011;134(Pt 11):e195.

8. Carelli V, Musumeci O, Caporali L, et al. Syndromic parkinsonism and dementia associated with OPA1 missense mutations. *Ann Neurol*. 2015;78:21.

9. Del Dotto V, Fogazza M, Musiani F, et al. Deciphering OPA1 mutations pathogenicity by combined analysis of human, mouse and yeast cell models. *Biochim Biophys Acta Mol Basis Dis*. 2018;1864:3496–3514.

10. Lodi R, Tonon C, Valentino ML, et al. Defective mitochondrial adenosine triphosphate production in skeletal muscle from patients with dominant optic atrophy due to OPA1 mutations. *Arch Neurol*. 2011;68:67–73.

11. Zanna C, Ghelli A, Porcelli AM, et al. OPA1 mutations associated with dominant optic atrophy impair oxidative phosphorylation and mitochondrial fusion. *Brain*. 2008;131:352–367.

12. Yu-Wai-Man P, Shankar SP, Biousse V, et al. Genetic screening for OPA1 and OPA3 mutations in patients with suspected inherited optic neuropathies. *Ophthalmology*. 2011;118:558–563.

13. Burté F, Carelli V, Chinnery PF, Yu-Wai-Man P. Disturbed mitochondrial dynamics and neurodegenerative disorders. *Nat Rev Neurol*. 2015;11:11–24.

14. Sarzi E, Angebault C, Seveno M, et al. The human OPA1delTTAG mutation induces premature age-related systemic neurodegeneration in mouse. *Brain*. 2012;135:3599–3613.

15. Wai T, García-Prieto J, Baker MJ, et al. Imbalanced OPA1 processing and mitochondrial fragmentation cause heart failure in mice. *Science*. 2015;350.

16. Dorn GW, Clark CF, Eschenbacher WH, et al. MARF and Opa1 control mitochondrial and cardiac function in *Drosophila*. *Circ Res*. 2011;108:12–17.

17. Shahrestani P, Leung H-T, Le PK, et al. Heterozygous mutation of *Drosophila* Opa1 causes the development of multiple organ abnormalities in an age-dependent and organ-specific manner. *PLoS One*. 2009;4:6867.

18. Bhandari P, Song M, Dorn GW. Dissociation of mitochondrial from sarcoplasmic reticular stress

in *Drosophila* cardiomyopathy induced by molecularly distinct mitochondrial fusion defects. *J Mol Cell Cardiol*. 2015;80:71–80.

19. Piquereau J, Caffin F, Novotova M, et al. Down-regulation of OPA1 alters mouse mitochondrial morphology, PTP function, and cardiac adaptation to pressure overload. *Cardiovasc Res*. 2012;94:408–417.

20. Kasahara A, Cipolat S, Chen Y, Dorn GW, Scorrano L. Mitochondrial fusion directs cardiomyocyte differentiation via calcineurin and Notch signaling. *Science*. 2013;342:734–737.

21. Chen L, Gong Q, Stice JP, Knowlton AA. Mitochondrial OPA1, apoptosis, and heart failure. *Cardiovasc Res*. 2009;84:91–99.

22. Yu J, Maimaitili Y, Xie P, et al. High glucose concentration abrogates sevoflurane postconditioning cardioprotection by advancing mitochondrial fission but dynamin-related protein 1 inhibitor restores these effects. *Acta Physiol (Oxf)*. 2017;220:83–98.

23. Yu-Wai-Man P, Griffiths PG, Gorman GS, et al. Multi-system neurological disease is common in patients with OPA1 mutations. *Brain*. 2010;133:771–786.

24. Yu-Wai-Man P, Votruba M, Burté F, Morgia C La, Barboni P, Carelli V. A neurodegenerative perspective on mitochondrial optic neuropathies. *Acta Neuropathol*. 2016;132:789.

25. Lee J, Jung SC, Hong Y Bin, et al. Recessive optic atrophy, sensorimotor neuropathy and cataract associated with novel compound heterozygous mutations in OPA1. *Mol Med Rep*. 2016;14:33.

26. Maeda-Katahira A, Nakamura N, Hayashi T, et al. Autosomal dominant optic atrophy with OPA1 gene mutations accompanied by auditory neuropathy and other systemic complications in a Japanese cohort. *Mol Vis*. 2019;25:559.

27. Othman BAL, Ong JE, Dumitrescu AV. Biallelic optic atrophy 1 (OPA1) related disorder—case report and literature review. *Genes*. 2022;13:1005.

28. Lindeberg J, Usoskin D, Bengtsson H, et al. Transgenic expression of Cre recombinase from the tyrosine hydroxylase locus. *Genesis*. 2004;40:67–73.

29. Cogliati S, Frezza C, Soriano ME, et al. Mitochondrial cristae shape determines respiratory chain supercomplexes assembly and respiratory efficiency. *Cell*. 2013;155:160–171.

30. Donadio V, Incensi A, Giannoccaro MP, et al. Peripheral autonomic neuropathy: diagnostic contribution of skin biopsy. *J Neuropathol Exp Neurol*. 2012;71:1000–1008.

31. Finsterer J, Laccone F. Autosomal dominant optic atrophy plus due to the novel OPA1 variant c.1463G>C. *Metab Brain Dis*. 2019;34:1023–1027.

32. Amati-Bonneau P, Valentino ML, Reynier P, et al. OPA1 mutations induce mitochondrial DNA instability and optic atrophy "plus" phenotypes. *Brain*. 2008;131:338–351.

33. Del Dotto V, Mishra P, Vidoni S, et al. OPA1 Isoforms in the Hierarchical Organization of Mitochondrial Functions. *Cell Rep*. 2017;19:2557–2571.

34. Zaglia T, Milan G, Franzoso M, et al. Cardiac sympathetic neurons provide trophic signal to the heart via β2-adrenoceptor-dependent regulation of proteolysis. *Cardiovasc Res*. 2013;97:240–250.

35. Hasan W. Autonomic cardiac innervation: Development and adult plasticity. *Organogenesis*. 2013;9:176.

36. Pianca N, Di Bona A, Lazzeri E, et al. Cardiac sympathetic innervation network shapes the myocardium by locally controlling cardiomyocyte size through the cellular proteolytic machinery. *J Physiol*. 2019;597:3639–3656.

37. Ye M, Lehigh KM, Ginty DD. Multivesicular bodies mediate long-range retrograde NGF-TrkA signaling. *Elife*. 2018;7.

38. Conroy JN, Coulson EJ. High-affinity TrkA and p75 neurotrophin receptor complexes: a twisted affair. *J Biol Chem*. 2022;298:101568.

39. Heerssen HM, Pazyra MF, Segal RA. Dynein motors transport activated Trks to promote survival of target-dependent neurons. *Nat Neurosci*. 2004;7:596–604.

40. Ginty DD, Segal RA. Retrograde neurotrophin signaling: Trk-ing along the axon. *Curr Opin Neurobiol*. 2002;12:268–274.

41. Mattson MP, Wan R. Neurotrophic factors in autonomic nervous system plasticity and dysfunction. *NeuroMolecular Med*. 2008;10:157–168.

42. Mattson MP, Gleichmann M, Cheng A. Mitochondria in neuroplasticity and neurological disorders. *Neuron*. 2008;60:748–766.

43. Pernas L, Scorrano L. Mito-morphosis: mitochondrial fusion, fission, and cristae remodeling as key mediators of cellular function. *Annu Rev Physiol*. 2016;78:505–531.

44. Favaro G, Romanello V, Varanita T, et al. DRP1-mediated mitochondrial shape controls calcium homeostasis and muscle mass. *Nat Commun*. 2019;10:2576.

45. Frezza C, Cipolat S, Martins de Brito O, et al. OPA1 controls apoptotic cristae remodeling independently from mitochondrial fusion. *Cell*. 2006;126:177–189.

46. Zaglia T, Mongillo M. Cardiac sympathetic innervation, from a different point of (re)view. *Physiol Soc*. 2017;595:3919–3930.

47. Prando V, Da Broi F, Franzoso M, et al. Dynamics of neuroeffector coupling at cardiac sympathetic synapses. *J Physiol*. 2018;596:2055–2075.

48. Dokshokova L, Franzoso M, Bona A Di, et al. Nerve growth factor transfer from cardiomyocytes to innervating sympathetic neurons activates TrkA receptors at the neuro-cardiac junction. *J Physiol*. 2022. https://doi.org/10.1113/JP28282

49. Franzoso M, Dokshokova L, Vitiello L, Zaglia T, Mongillo M. Tuning the consonance of microscopic neuro-cardiac interactions allows the heart beats to play countless genres. *Front Physiol*. 2022;13.

50. Oettinghaus B, Schulz JM, Restelli LM, et al. Synaptic dysfunction, memory deficits and hippocampal atrophy due to ablation of mitochondrial fission in adult forebrain neurons. *Cell Death Differ*. 2016;23:18–28.

51. Guo T, Zhang D, Zeng Y, Huang TY, Xu H, Zhao Y. Molecular and cellular mechanisms underlying the pathogenesis of Alzheimer's disease. *Mol Neurodegener*. 2020;15.

52. Jadiya P, Garbincius JF, Elrod JW. Reappraisal of metabolic dysfunction in neurodegeneration: Focus on mitochondrial function and calcium signaling. *Acta Neuropathol Commun*. 2021;9.

53. Von Stockum S, Sanchez-Martinez A, Corrà S, et al. Inhibition of the deubiquitinase USP8 corrects a *Drosophila* PINK1 model of mitochondria dysfunction. *Life Sci alliance*. 2019;2.

54. Wauters F, Cornelissen T, Imberechts D, et al. LRRK2 mutations impair depolarization-induced mitophagy through inhibition of mitochondrial accumulation of RAB10. *Autophagy*. 2020;16:203–222.

55. Liu C, Fu Z, Wu S, et al. Mitochondrial HSF1 triggers mitochondrial dysfunction and neurodegeneration in Huntington's disease. *EMBO Mol Med*. 2022;14.

56. Alqahtani T, Deore SL, Kide AA, et al. Mitochondrial dysfunction and oxidative stress in Alzheimer's disease, and Parkinson's disease, Huntington's disease and amyotrophic lateral sclerosis – an updated review. *Mitochondrion*. 2023;71:83–92.

57. Jhanji R, Behl T, Sehgal A, Bungau S. Mitochondrial dysfunction and traffic jams in amyotrophic lateral sclerosis. *Mitochondrion*. 2021;58:102–110.

58. Muyderman H, Chen T. Mitochondrial dysfunction in amyotrophic lateral sclerosis – a valid pharmacological target? *Br J Pharmacol*. 2014;171:2191–2205.

59. Tammineni P, Ye X, Feng T, Aikal D, Cai Q. Impaired retrograde transport of axonal autophagosomes contributes to autophagic stress in Alzheimer's disease neurons. *Elife*. 2017;6.

60. Moller A, Bauer CS, Cohen RN, Webster CP, De Vos KJ. Amyotrophic lateral sclerosis-associated mutant SOD1 inhibits anterograde axonal transport of mitochondria by reducing Miro1 levels. *Hum Mol Genet*. 2017;26:4668–4679.

61. Sung H, Lloyd TE. Defective axonal transport of endo-lysosomes and dense core vesicles in a *Drosophila* model of C9-ALS/FTD. *Traffic*. 2022;23:430–441.

62. Sleigh JN, Tosolini AP, Gordon D, et al. Mice carrying ALS mutant TDP-43, but not mutant

FUS, display in vivo defects in axonal transport of signaling endosomes. *Cell Rep*. 2020;30:3655–3662.e2.

63. Kulkarni VV, Stempel MH, Anand A, Sidibe DK, Maday S. Retrograde axonal autophagy and endocytic pathways are parallel and separate in neurons. *J Neurosci*. 2022;42:8524–8541.

64. Boecker CA, Goldsmith J, Dou D, Cajka GG, Holzbaur ELF. Increased LRRK2 kinase activity alters neuronal autophagy by disrupting the axonal transport of autophagosomes. *Curr Biol*. 2021;31:2140–2154.e6.

65. Shlevkov E, Kramer T, Schapansky J, Lavoie MJ, Schwarz TL. Miro phosphorylation sites regulate Parkin recruitment and mitochondrial motility. *Proc Natl Acad Sci U S A*. 2016;113:E6097–E6106.

66. Brady ST, Morfini GA. Regulation of motor proteins, axonal transport deficits and adult-onset neurodegenerative diseases. *Neurobiol Dis*. 2017;105:273–282.

KEY WORDS dominant optic atrophy, mitochondria, nerve growth factor, optic atrophy factor-1, sympathetic neurons

APPENDIX For supplemental methods, references, tables, and a figure, please see the online version of this paper.